IOP Publishing New J. Phys. 25 (2023) 113039 https://doi.org/10.1088/1367-2630/ad0c84

New Journal of Physics
The open access journal at the forefront of physics

Deutsche Physikalische Gesellschaft DPG
IOP Institute of Physics
Published in partnership with: Deutsche Physikalische Gesellschaft and the Institute of Physics

OPEN ACCESS

RECEIVED
23 August 2023

REVISED
31 October 2023

ACCEPTED FOR PUBLICATION
14 November 2023

PUBLISHED
23 November 2023

PAPER

Demonstration of reversed non-Hermitian skin effect via quantum walks on a ladder

Xiaowei Wang[1], **Lei Xiao**[2,1], **Quan Lin**[1], **Kunkun Wang**[3], **Haiqing Lin**[4] and **Peng Xue**[2,1,*]

[1] Beijing Computational Science Research Center, Beijing 100084, People's Republic of China
[2] School of Physics, Southeast University, Nanjing 211189, People's Republic of China
[3] School of Physics and Optoelectronic Engineering, Anhui University, Hefei 230601, People's Republic of China
[4] School of Physics, Zhejiang University, Hangzhou 310030, People's Republic of China
[*] Author to whom any correspondence should be addressed.

E-mail: gnep.eux@gmail.com

Keywords: quantum walks, non-Hermitian, reversed non-Hermitian skin effect

Abstract

Quantum walks hold enormous potential applications in various areas such as quantum computing and quantum simulation. Discrete-time quantum walks on a ladder offer greater prospects compared to traditional quantum walks, especially in addressing physical problems in higher-dimension coupled systems. Here we give an experimental proposal of quantum walks on a two-leg ladder using linear optics, and further apply it to non-Hermitian systems by introducing loss-based non-unitary evolutions. Non-Hermitian systems under nonreciprocity-induced evolution present an exotic phenomenon, known as the non-Hermitian skin effect (NHSE). In a two-leg non-Hermitian system with the same preferred direction of NHSE, the direction has recently been found to reverse when interchain couplings are introduced. Based on quantum walks on a ladder, we also propose an experimentally feasible scheme to demonstrate the direction reversal of NHSE. Through the simulated results we show that particles on each chain accumulate to the preferred boundary driven by nonreciprocal hopping, while particles are transported in the opposite direction when interchain hopping is allowed, clearly demonstrating the existence of reversed NHSE. Our work further expands the application of the quantum walk platform and opens a door for the experimental investigation of reversed NHSE.

1. Introduction

Since quantum walks was proposed by Aharonov *et al* [1], relevant research has made significant progress, primarily focusing on two major research areas. First, from the perspective of quantum computing, quantum walks have been studied in solving quantum problems such as cellular automata [2], quantum search algorithms [3, 4] and universal quantum computation [5]. Secondly, quantum walks have been explored as a tool for quantum simulation in studying various physical problems, including topological phases [6, 7], Anderson localization, decoherence [8–10] and others. In addition, experimental schemes for implementing quantum walks have also been proposed, such as experiments with ions [11], atoms [12], and photons [13–17].

The dynamics of quantum walks are described by iterating a unitary time-step operator, where the dynamical process of quantum walk can be considered as the simulation of time evolution governed by the effective Hamiltonian H_{eff}, i.e. $U = e^{-iH_{\mathrm{eff}}}$ [16]. In this sense, quantum walks serve as an effective method of simulating Hamiltonian H_{eff} with a quantum flash simulator. This is a powerful theoretical concept that allows for the application of many physical intuitions about lattice systems to quantum walks. Compared to traditional one-dimension quantum walks, the quantum walks on a ladder need to connect two one-dimension quantum walks and offer greater application prospects [18]. Indeed, it is an interesting example of two-dimensional quantum walks. In this paper, we focus on a experimental scheme of quantum walks on a two-leg ladder and its application in a coupled double-chain non-Hermitian lattice model by introducing loss-based non-unitary evolutions. Recently, two-dimensional quantum walks has been implemented by different photonic platforms, including continuous-time quantum walks [19–21] and discrete-time quantum walks [22–25]. Most of these methods are implemented using integrated photonics. Their platforms are small in size and highly integrated. However, there are also some challenges, such as complex manufacturing and limited adjustability due to their fixed structures. Compared to these methods, our scheme is based on bulk optics implementations, which is composed of linear optical elements that are easier to manipulate and expand. Therefore, the bulk optics we use can overcome these difficulties and has the advantages of high flexibility and strong adjustability, which further expands its application scope and can be applied to different optical fields. In fact, the two methods can also be organically combined and converted [26]. Our method also provides a good reference for using integrated photonics to study non-Hermitian physics via quantum walks on the two-leg ladder.

Following the discoveries of non-Hermitian Hamiltonians in physical systems [27–30], a wealth of intriguing physical phenomena and applications have been explored [31–44]. In the non-Hermitian lattice system with nonreciprocity, the non-Hermitian skin effect (NHSE) describes the phenomenon of localization of eigenstates under the open boundary condition (OBC) [45]. These phenomena are not the same as Hermitian topological systems thus have attracted much attention recently, such as new theories to interpret NHSE and describe the related topological properties [46–54], extensions of NHSE from one dimension to higher dimensions [55–58], and experimental demonstration of the NHSE [16, 59–63]. In one-dimensional non-Hermitian lattice, the skin modes are generally localized in the preferred direction of particle accumulation. The preferred direction is associated with nonreciprocal hopping. If the hopping strength between the right and left is unequal, particles are ready to accumulate in the direction where the hopping strength is greater. The directional transport caused by nonreciprocity-induced non-Hermiticity has great application prospects for other dynamics. Recently, Li *et al* [64] proposed the reversed NHSE with the opposite direction to the preferred direction in the Hatano–Nelson (HN) chains. In a double-chain HN model with nonreciprocal hopping, the direction of the NHSE is reversed by introducing interchain coupling. Studies of nonreciprocal transmission and reversed NHSE show theoretical interest and application prospects [59, 65, 66]. As is well-known, the NHSE has been observed in some experimental platforms, such as linear optical systems, optomechanical systems, superconducting circuits, and topolectric circuits [16, 59–63, 67–71], which gives us a good inspiration to experimentally study reversed NHSE with a quantum walk platform.

In this paper, unlike previous discussions in [64] that focused on the dynamics of quantum walks, we primarily investigate the topic from the perspective of the effective Hamiltonian H_{eff} of quantum walks, which is a key factor for analyzing quantum dynamics. We compute and analyze the effective Hamiltonian along with its corresponding topological phase diagram. Additionally, we introduce a more intuitive physical quantity, the mean center of mass of the system, to characterize the degree of inversion. These further enhance our understanding of topological property and the reversed behavior in quantum walks at its core. Moreover, we provide the concrete and feasible experimental proposal based on the idea of the quantum walk on a ladder, thereby making the study of reversed NHSE more practically significant. Here we propose a specific scheme using linear optics to demonstrate the reverse NHSE via a non-unitary quantum walk on a ladder. To simulate the non-Hermitian quasicrystal with interchain coupling, we consider a quantum walk on a ladder governed by a $2 \times 2 \times n$ Floquet operator. Interchain coupling and nearest neighbor hopping can be achieved by the walker changing the leg of the ladder. Without interchain hopping, the eigenmodes are accumulated at the right boundary. Whereas, when interchain hopping is introduced, a reversal of direction occurs, and the localization direction of eigenmodes is towards the left boundary. Our proposal is experimentally feasible with the current technologies and can be extended in future studies of non-Hermitian quasicrystals with coherent coupling.

2. Protocol of quantum walks on a ladder and linear optical realization

Here we study the discrete-time quantum walk. For one-dimension quantum walk, the probability distribution spreads at each step along a straight line. In higher dimensions, the distribution can further expand in different directions depending on the predetermined protocol, such as quantum walks on a cylinder [72] or on graphs [73]. Here, we focus on a specific type of quantum walks called quantum walks on a ladder, which involves connecting two one-dimensional quantum walks together, as shown in figure 1(a). The Hilbert space of the system can be expressed as the tensor product space of two legs, spatial sites and the coins $\mathcal{H} = \mathcal{H}_{\mathrm{leg}} \otimes \mathcal{H}_{\mathrm{site}} \otimes \mathcal{H}_{\mathrm{coin}}$. The state of the walker is typically labeled by its leg position $|y\rangle$, site position $|x\rangle$. The coin state $|u\rangle$ denotes the state of the single qubit, which can choose the spin state (spin up, spin down), vertical polarization, horizontal polarization or their mixture.

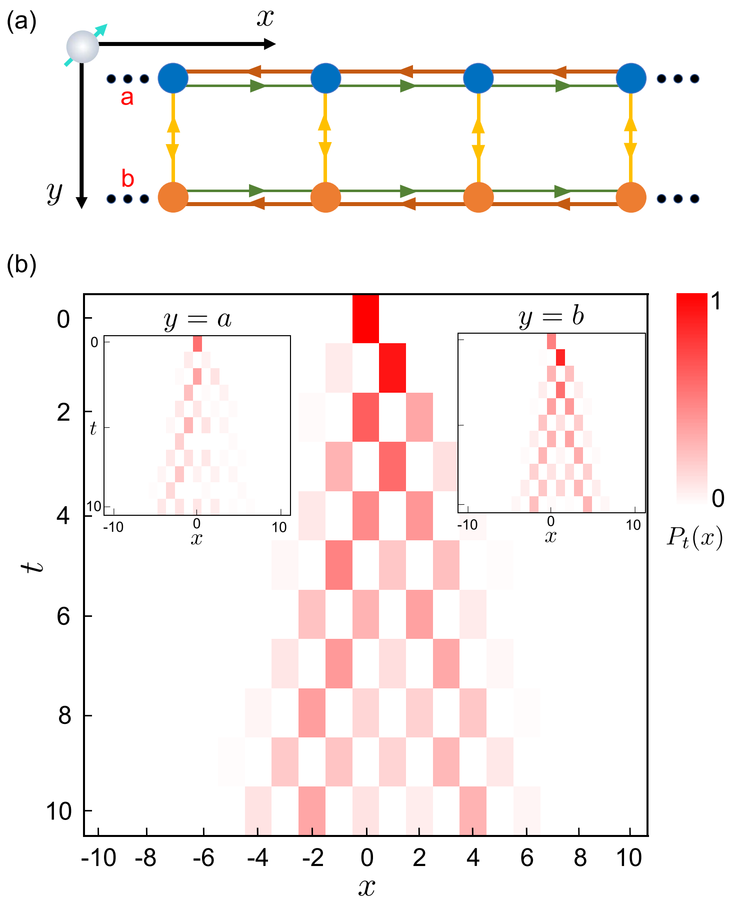

Figure 1. (a) The diagram of quantum walks on a two-leg ladder. The particle moves up and down or left and right depending on its coin state. (b) The normalized spatial probability distributions $P_t(x) = P_t^a(x) + P_t^b(x)$. Insets: the spatial probability distributions of different site position x on leg a or leg b: $P_t^a(x)$ or $P_t^b(x)$, respectively. The initial state of the walker is prepared as $|\Phi_0\rangle = \sum_{x,y=a,b,u=0,1} \phi_0^{y,x,u} |y,x\rangle \otimes |u\rangle$ with normalized factor $\phi_0^{y,x,u}$. Here we choose $x = 0$, $u = 0$ and $\phi_0^{a,0,0} = \phi_0^{b,0,0} = 1/\sqrt{2}$, i.e. $|\Phi_0\rangle = (|a,0\rangle \otimes |0\rangle + |b,0\rangle \otimes |0\rangle)/\sqrt{2}$. Other parameters: $\theta = 0.25\pi$ and $\theta_\uparrow = \theta_\downarrow = 0.5\pi$.

First, we consider a conventional discrete-time quantum walk along a straight line in the x direction, governed by the operator $U_x^{\text{line}} = S_x C(\theta)$ with the shift operators

$$S_x = \sum_x \sum_y |y,x+1\rangle\langle y,x| \otimes |0\rangle\langle 0| + |y,x-1\rangle\langle y,x| \otimes |1\rangle\langle 1|, \tag{1}$$

and the coin operator

$$C(\theta) = \sum_x \sum_y |y,x\rangle\langle y,x| \otimes e^{-i\theta\sigma_2/2}.$$

Here $\sigma_{1,2,3}$ are the standard Pauli matrices. The coin states $|0\rangle$ and $|1\rangle$ are the eigenstates of the Pauli matrix σ_3. For quantum walks on a ladder, we need special shift operators so that walkers can hop between the two legs. The unitary evolution for hopping between the two legs is $U_y^{\text{leg}} = S_\uparrow C(\theta_\uparrow) S_\downarrow C(\theta_\downarrow)$ with

$$\begin{aligned} S_\downarrow &= \sum_y \sum_x |y,x\rangle\langle y,x| \otimes |1\rangle\langle 1| + |y-1,x\rangle\langle y,x| \otimes |0\rangle\langle 0|, \\ S_\uparrow &= \sum_y \sum_x |y,x\rangle\langle y,x| \otimes |0\rangle\langle 0| + |y+1,x\rangle\langle y,x| \otimes |1\rangle\langle 1|, \end{aligned} \tag{2}$$

The goal is to keep walkers on both sides of the ladder, hence we combine the two kinds of walking evolution, one step evolution on the ladder are governed by this Floquet operator

$$U = U_y^{\text{leg}} U_x^{\text{line}} = S_\uparrow C(\theta_\uparrow)\, S_\downarrow C(\theta_\downarrow)\, S_x C(\theta)\,. \tag{3}$$

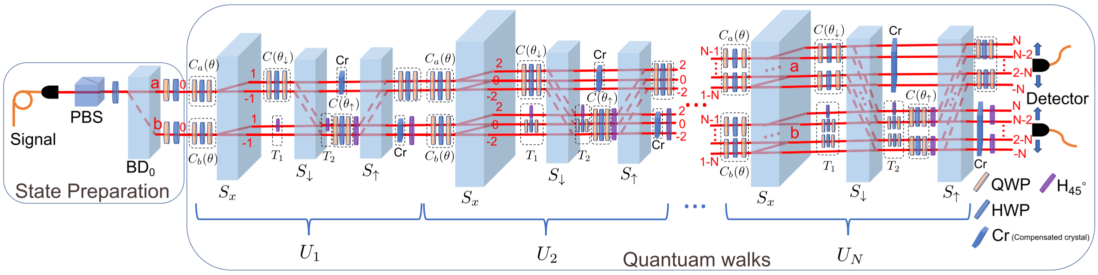

Figure 2. Schematic of experimental setup. The signal photon is injected into the subsequent interferometric network. The parameters of the initial states are controlled via the setting angles of three half-wave plates (HWPs), two quarter-wave plates (QWPs) and a beam displacer (BD) followed by a polarizing beam splitter (PBS). Here BD$_0$ is used to stratify the leg into upper and lower legs. We define the upper path as the leg a and the lower as the leg b, respectively. The unitary evolutions U are realized by a set of wave plates and an interferometer involving two BDs. After state preparation, the solid lines inside BDs represent their respective intrachain hopping for each leg, and dotted lines represent interchain hopping between two legs. The compensated crystal (Cr) here is used to compensate the undesired optical path length difference between the different paths. The total time step of quantum walks is taken $t = N$. Output photons are detected by the avalanche photodiodes (APDs).

The evolved state after t step is expressed as $|\Phi_t\rangle = U_t \cdots U_2 \cdot U_1 |\Phi_0\rangle = U^t |\Phi_0\rangle$. In figure 1(a), we show a simple two-leg ladder diagram ($y = a, b$) where walkers can stay on both sides of the ladder. In order to ensure the unitary evolution, the boundary conditions are applied in the y direction. Here we specify that the particles which will hop beyond the y boundary in the next step do not jump up or down, and they still stay at the original site position. Consider this simple case of a quantum walker moving on a ladder, we obtain the spatial probability distributions in figure 1(b). We find the probability amplitudes spread rapidly on two legs. Compared with traditional quantum walks, using specific protocols for walking on the ladder provides the walker with additional options for walking and extends the time and space resources available to walkers, which will have greater application prospects.

In general, the lossless experimental setup can be described by a unitary operator, and here we present a simple and general method for designing experimental implementations of quantum walks on the two-leg ladder. We use the optical arrangement of BDs, polarization beam splitters, phase shifters and polarization wave plates to move the heralded single photon to each location on the ladder according to the walking protocol. It should be mentioned that it does not matter what field we use here. We chose photons here for the convenience of discussion, because high-power sources, even entangled radiation, are available [74]. However, we note that it is equally possible to achieve optical circuits for electrons, atoms, or any other type of radiation.

As shown in figure 2, the whole scheme is mainly composed of three parts: preparation of system initial state, implementation of evolution operator, and measurement. The heralded single photons can be injected into photonic circuits. Then one of these yielded pairs of photons is heralded as a signal photon into the subsequent interferometric network, and the other serves as a trigger. For initial quantum state preparation, the heralded single photons first pass through a polarizing beam splitter (PBS) and a half-wave plate (HWP). The polarization states $|H\rangle = (1,0)^{\mathrm{T}}$ and $|V\rangle = (0,1)^{\mathrm{T}}$ can be arbitrarily rotated using a combination of two quarter-wave plates (QWPs) at φ and an HWP at ϑ, where the rotation operator

$$C(\theta) = R_{\mathrm{QWP}}(\varphi_1) \cdot R_{\mathrm{HWP}}(\vartheta) \cdot R_{\mathrm{QWP}}(\varphi_2) \tag{4}$$

with the unitary matrix forms

$$R_{\mathrm{QWP}}(\varphi) = \begin{pmatrix} \cos^2\varphi + i\sin^2\varphi & (1-i)\sin\varphi\cos\varphi \\ (1-i)\sin\varphi\cos\varphi & \sin^2\varphi + i\cos^2\varphi \end{pmatrix},$$

and

$$R_{\mathrm{HWP}}(\vartheta) = \begin{pmatrix} \cos 2\vartheta & \sin 2\vartheta \\ \sin 2\vartheta & -\cos 2\vartheta \end{pmatrix},$$

respectively. We can implement any rotation operator with three wave plates (QWP-HWP-QWP), only one or two wave plates are generally required in practice. The optical axis of beam displacers (BDs) is cut so that the vertically polarized photons are transmitted directly and the horizontally polarized photons are displaced into a neighboring spatial mode. Then the photons are separated into two paths by a birefringent calcite beam displacer (BD$_0$). Here we define the upper path as leg a and the lower as leg b, and the site positions of the walker on both legs are initialized to $x_0 = 0$. The initial state is $|\Phi_0\rangle = \sum_{x,y=a,b,u=0,1} \phi_0^{y,x,u} |y,x\rangle \otimes |u\rangle$ with normalized factor $\phi_0^{y,x,u}$ determined by the angles of five wave plates close to (BD_0), $u = |H\rangle, |V\rangle$ denoting the polarized state.

To implement the operator U_x^{line}, the shift operator S_x can be realized by BDs, and the coin rotation operator $C(\theta)$ can be realized by three wave plates (QWP-HWP-QWP). It should be noted that the optical axes of the BDs realizing S_x should be perpendicular to that of the first BD_0. After passing through these BDs realizing S_x, the photons on each leg are independently divided into the front and back paths depending on their polarization states, realizing photons' hopping between site positions on respective leg where moving forward $x + 1$ corresponds to $|H\rangle$ and moving backwards $x - 1$ corresponds to $|V\rangle$.

The experimental implementation of the operator U_y^{leg} is similar to that of U_x^{line} except for interchain shift operators $S_\uparrow$ and $S_\downarrow$, as shown in figure 2. The operators $C(\theta_\uparrow)$ and $C(\theta_\downarrow)$ are implemented as well as $C(\theta)$. The operators $S_\uparrow$ and $S_\downarrow$ are introduced to couple the upper leg a and lower leg b. The optical axis of placed BDs realizing $S_\uparrow$ and $S_\downarrow$ should be parallel to that of the BD_0 originally used to generate leg layering. Therefore, the photons of the same site position index x hop up and down from one leg to another controlled by their polarization states, i.e. the photons hop up from $|b,x\rangle$ to $|a,x\rangle$ and down from $|a,x\rangle$ to $|b,x\rangle$. The compensated crystals here are inserted on these appropriate paths to compensate the undesired optical path length difference between the different paths [75], ensuring that all optical paths that need to interference are of the same length.

To realize the mutual interchain hopping between two legs, we also need to consider the boundary conditions. Two BDs are respectively needed to achieve $S_\uparrow$ and $S_\downarrow$, and the design of the optical path combines with coin rotation operators $C(\theta_\uparrow)$ and $C(\theta_\downarrow)$. We first realize the hopping from leg a to leg b and then realize the hopping from leg b to leg a. During this process, the operator T_1 is used here, and its expression is as follows

$$T_1 = \sum_x \sum_{y=a,b} |y,x\rangle\langle y,x| \otimes \begin{pmatrix} e^{-i(\xi+\zeta)/2}\cos\varpi/2 & -e^{-i(\xi-\zeta)/2}\sin\varpi/2 \\ e^{i(\xi-\zeta)/2}\sin\varpi/2 & e^{i(\xi+\zeta)/2}\cos\varpi/2 \end{pmatrix}, \tag{5}$$

where the second term of equation (5) represents the general form of the $SU(2)$ matrix with ξ, ζ, ϖ as Euler angle parameters. The operator T_1 can rotate any polarization state into another and $C(\theta)$ is just its subgroup of $SU(2)$ [76]. Similarly, the operator T_1 is experimentally easy to be implemented by three wave plates (QWP-HWP-QWP). We rotate these wave plates' angles of the operator T_1 to make the related photons' polarization states completely into $|V\rangle$, ensuring that horizontally polarized photons on the leg b cannot jump out of the boundary in the y direction while the shift operator $S_\downarrow$ acts. When there is a single coin state $|H\rangle$ on site positions, we only need to use a HWP at 45°. After passing through two BDs, the operator T_2 is used to eliminate the effect of T_1 transformation and the exchange of $|H\rangle$ and $|V\rangle$ on the evolved states. If we consider their matrix forms, they satisfy the relation $T_1 T_2 = \mathbb{1}$. The purpose of the T_1 and T_2 setting here is to ensure that the boundary conditions are met. Especially, when realizing the shift operator $S_\uparrow$ which controls the hopping of photons only in a vertically polarized state, we can operate it by using an HWP at 45° to turn $|V\rangle$ into $|H\rangle$, and then add the same HWP for transformation back for the leg b. For the leg a we add three wave plates for transformation back into $|V\rangle$. The theoretical angles of the wave plates are mentioned above can also be calculated according to the preceding coin states. In addition, operators T_1 and T_2 can also be used to adjust the hopping strength between the upper and lower leg depending on the needs of the experiment.

Then the walkers iteratively evolve step by step. After every time step, photons are detected by the detectors, recording photons coincidence events. Through measurement we can obtain the number of photons of leg a and leg b at different positions $n_t^{x,y}$ and their sum is the total number of photons n_t after t steps. Experimentally, we can obtain $P_t(x) = (\sum_{y=a,b} n_t^{x,y})/n_t$ or other observable quantities, further demonstrating the feasibility of the experimental scheme.

According to the above discussion and figure 2, when the site positions take $x = -N \ldots N$, we can obtain the expression between the number of BDs and the position of the walker after the whole evolution: number (BD) $= 3N$, where the BD used for state preparation is not considered, and the quantitative relation between the optical depth of cascade interferometers and the position of the walker

$$\mathrm{OD} = 3N - 1. \tag{6}$$

In fact, even if the lattice positions are not extended, the number of BDs implementing the one-step evolution obeys a linear polynomial function due to the properties of quantum walks on a ladder and experimental devices. We thus obtain that the number of BDs obeys a linear function with the positional scale of the quantum system. In some experimental schemes, the similar relationship tends to change quadratically as function of N [77, 78]. Besides that, the relationship between the optical depth and the positional scale of the quantum system also obeys a linear function in our scheme. These results confirm that our proposed optical circuits have the low complexity of and is easier to implement.

3. Reversed NHSE in quantum walks on a ladder

The NHSE is often related to nonreciprocity, and usually occurs in a system with on-site gain/loss. To uncover the propagation mechanism of particle accumulation on the quantum dynamics level, we present a proposal to observe and understand the reversed NHSE in the quantum-walk dynamics driven by a non-unitary topological Floquet operator.

First, we consider a two-leg discrete-time quantum walk without hopping between legs, governed by this Floquet operator

$$U_0 = C(\theta_1)\,S_2 C(\theta_0)\,MC(\theta_0)\,S_1 C(\theta_1) \tag{7}$$

with the shift operators

$$\begin{aligned} S_1 &= \sum_x \sum_{y=a,b} |y,x\rangle\langle y,x| \otimes |1\rangle\langle 1| + |y,x+1\rangle\langle y,x| \otimes |0\rangle\langle 0|, \\ S_2 &= \sum_x \sum_{y=a,b} |y,x\rangle\langle y,x| \otimes |0\rangle\langle 0| + |y,x-1\rangle\langle y,x| \otimes |1\rangle\langle 1|, \end{aligned}$$

and the coin rotation operator $C(\theta) = \sum_x \sum_{y=a,b} |y,x\rangle\langle y,x| \otimes e^{-i\lambda_y \theta \sigma_2/2}$, where the walker's position is labeled by x, and $y = a, b$ denotes the two legs of the ladder and $\lambda_a = -\lambda_b = 1$. Note that the form of this operator U_0 here slightly differs from the previous basic model because the various symmetries of the lattice structure are considered. Particles jump in both directions at once driven by the shift operators S_x, but here particles jump in one direction driven by the operators S_1 and S_2. Non-unitarity is introduced by the gain-loss operator with $M = \sum_x \sum_{y=a,b} |y,x\rangle\langle y,x| \otimes (|1\rangle\langle 1| + e^{-\eta}|0\rangle\langle 0|)$.

To investigate the effect of interchain coupling on the direction of NHSE, we couple the two legs of the ladder by introducing two specific shift operators S_3 and S_4 correlated with interchain hopping, where these operators S_3 and S_4 are similar variations of operators $S_\uparrow$ and $S_\downarrow$. The new Floquet operator is then

$$U = C(\theta_1)\,S_2 C(\theta_2)\,S_4 C(\theta_3)\,MC(\theta_3)\,S_3 C(\theta_2)\,S_1 C(\theta_1) \tag{8}$$

with

$$\begin{aligned} S_3 &= \sum_x \sum_{y \neq y' \in \{a,b\}} |y,x\rangle\langle y',x| \otimes |0\rangle\langle 0| + |y,x\rangle\langle y,x| \otimes |1\rangle\langle 1|, \\ S_4 &= \sum_x \sum_{y \neq y' \in \{a,b\}} |y,x\rangle\langle y',x| \otimes |1\rangle\langle 1| + |y,x\rangle\langle y,x| \otimes |0\rangle\langle 0|. \end{aligned}$$

Note that S_3 and S_4 are different from $S_\uparrow$ and $S_\downarrow$ in that they make particles hop up and down between two legs at the same time. Here we take $\theta_2 + \theta_3 = \theta_0$. Under the effect of the two operators, depending on the coin state, the walker leaps from one leg to another and keeps the same site.

The dynamical process of quantum walk can be considered as the simulation of time evolution governed by the effective Hamiltonian H_{eff}, i.e. $U = e^{-iH_{\text{eff}}}$ [16, 63]. Starting from the Floquet operator U_0 without interchain coupling in the momentum space, we obtain

$$U_0(k) = \begin{pmatrix} U_0^a(k) & \mathbf{0} \\ \mathbf{0} & U_0^b(k) \end{pmatrix}, \tag{9}$$

where $U_0^a(k)$ and $U_0^b(k)$ correspond to momentum operators of the walker on the legs a and b, respectively. We first consider

$$U_0^a(k) = d_0\sigma_0 + id_1\sigma_1 + id_2\sigma_2 + id_3\sigma_3, \tag{10}$$

where

$$d_0 = \omega_+ \cos k \cos(\theta_1\lambda_a)\cos(\theta_0\lambda_a) - \omega_+ \sin(\theta_1\lambda_a)\sin(\theta_0\lambda_a) + i\omega_- \cos(\theta_1\lambda_a)\sin k,$$

$$d_1 = 0,$$

$$\begin{aligned}
&d_2 = -\omega_+ \cos k \sin(\theta_1\lambda_a)\cos(\theta_0\lambda_a) - \omega_+ \cos(\theta_1\lambda_a)\sin(\theta_0\lambda_a) - i\omega_- \sin(\theta_1\lambda_a)\sin k,\\
&d_3 = -\omega_+ \sin k \cos(\theta_0\lambda_a) + i\omega_- \cos k,
\end{aligned} \tag{11}$$

and $\omega_\pm = (1 \pm e^{-\eta})/2$. When k approaches 0, d_3 is similar to the $\sin k + i\eta/2$ term which appears in the Su–Schrieffer–Heeger model with NHSE, which provides an intuitive understanding for NHSE [16, 45].

The effective Hamiltonian $H_{\mathrm{eff}}(k)$ can be defined through $H_{\mathrm{eff}}(k) = i\ln U(k)$, the right- and left-eigenvectors of $H_{\mathrm{eff}}(k)$ are the same as those of $U(k)$. Then we have $U_0^a(k)|\phi_\pm(k)\rangle = E_\pm(k)|\phi_\pm(k)\rangle$ and $U_0^{a\dagger}(k)|\chi_\pm(k)\rangle = E_\pm^*(k)|\chi_\pm(k)\rangle$. Here $E_\pm(k) = d_0 \pm D$ with $D = i\sqrt{d_1^2 + d_2^2 + d_3^2}$. We also have

$$\begin{aligned}
|\phi_\pm\rangle &= \frac{1}{\sqrt{-2D^2 \pm 2id_3D}}\begin{pmatrix} id_1 + d_2 \\ \pm D - id_3 \end{pmatrix},\\
|\chi_\pm\rangle &= \frac{1}{\sqrt{-2D^2 \pm 2id_3D}}\begin{pmatrix} id_1^* + d_2^* \\ \mp D^* - id_3^* \end{pmatrix}.
\end{aligned} \tag{12}$$

We can obtain

$$U_0^a(k) = E_+\frac{|\phi_+\rangle\langle\chi_+|}{\langle\chi_+|\phi_+\rangle} + E_-\frac{|\phi_-\rangle\langle\chi_-|}{\langle\chi_-|\phi_-\rangle}, \tag{13}$$

and it follows that $H_{0-\mathrm{eff}}^a(k)$ can be written as

$$H_{0-\mathrm{eff}}^a(k) = i\left[\ln(E_+)\frac{|\phi_+\rangle\langle\chi_+|}{\langle\chi_+|\phi_+\rangle} + \ln(E_-)\frac{|\phi_-\rangle\langle\chi_-|}{\langle\chi_-|\phi_-\rangle}\right]. \tag{14}$$

For the leg b, since there is no interchain coupling, we just replace λ_a by λ_b and follow the same calculation. Thus, we obtain the effective Hamiltonian of $U_0(k)$

$$H_{0-\mathrm{eff}}(k) = \begin{pmatrix} H_{0-\mathrm{eff}}^a(k) & 0 \\ 0 & H_{0-\mathrm{eff}}^b(k) \end{pmatrix}. \tag{15}$$

Next, we consider the Floquet operator U in equation (8) with interchain coupling in the momentum space. For the convenience of a more intuitive expression, the matrix decomposition is carried out according to whether there is an interchain coupling term,

$$U(k) = G_1(k)\,V(k)\,G_2(k), \tag{16}$$

where the uncoupled terms $G_1(k)$ and $G_2(k)$ are

$$G_1(k) = \begin{pmatrix} G_1^a(k) & \mathbf{0} \\ \mathbf{0} & G_1^b(k) \end{pmatrix}, G_2(k) = \begin{pmatrix} G_2^a(k) & \mathbf{0} \\ \mathbf{0} & G_2^b(k) \end{pmatrix}, \tag{17}$$

with

$$G_1^{a(b)}(k) = \begin{pmatrix} g_{11}^1 & g_{12}^1 \\ g_{21}^1 & g_{22}^1 \end{pmatrix}, G_2^{a(b)}(k) = \begin{pmatrix} g_{11}^2 & g_{12}^2 \\ g_{21}^2 & g_{22}^2 \end{pmatrix}, \tag{18}$$

where

$$\begin{aligned}
g_{11}^1 &= \cos\lambda_{a(b)}\theta_1/2\cos\lambda_{a(b)}\theta_2/2 - e^{ik}\sin\lambda_{a(b)}\theta_1/2\sin\lambda_{a(b)}\theta_2/2,\\
g_{12}^1 &= -\cos\lambda_{a(b)}\theta_1/2\sin\lambda_{a(b)}\theta_2/2 - e^{ik}\sin\lambda_{a(b)}\theta_1/2\cos\lambda_{a(b)}\theta_2/2,\\
g_{21}^1 &= \sin\lambda_{a(b)}\theta_1/2\cos\lambda_{a(b)}\theta_2/2 + e^{ik}\cos\lambda_{a(b)}\theta_1/2\sin\lambda_{a(b)}\theta_2/2,\\
g_{22}^1 &= -\sin\lambda_{a(b)}\theta_1/2\sin\lambda_{a(b)}\theta_2/2 + e^{ik}\cos\lambda_{a(b)}\theta_1/2\cos\lambda_{a(b)}\theta_2/2;\\
g_{11}^2 &= e^{-ik}\cos\lambda_{a(b)}\theta_1/2\cos\lambda_{a(b)}\theta_2/2 - \sin\lambda_{a(b)}\theta_1/2\sin\lambda_{a(b)}\theta_2/2,\\
g_{12}^2 &= -\cos\lambda_{a(b)}\theta_1/2\sin\lambda_{a(b)}\theta_2/2 - e^{-ik}\sin\lambda_{a(b)}\theta_1/2\cos\lambda_{a(b)}\theta_2/2,\\
g_{21}^2 &= \sin\lambda_{a(b)}\theta_1/2\cos\lambda_{a(b)}\theta_2/2 + e^{-ik}\cos\lambda_{a(b)}\theta_1/2\sin\lambda_{a(b)}\theta_2/2,\\
g_{22}^2 &= \cos\lambda_{a(b)}\theta_1/2\cos\lambda_{a(b)}\theta_2/2 - e^{-ik}\sin\lambda_{a(b)}\theta_1/2\sin\lambda_{a(b)}\theta_2/2.
\end{aligned}$$

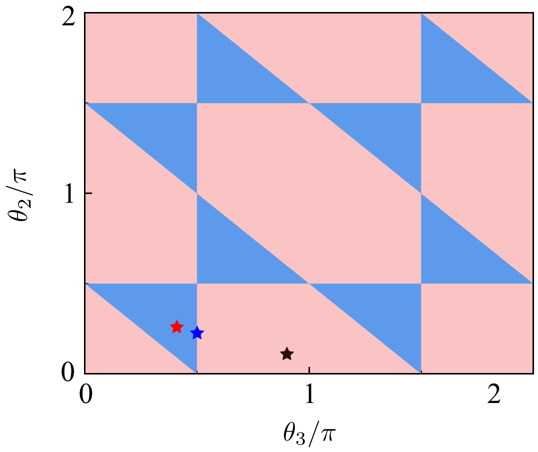

Figure 3. Topological phase diagram driven by $H_{\mathrm{eff}}(k)$. The blue and pink regions represent topological nontrivial regions with opposite topological numbers, and the region along phase boundaries represents trivial topology. The star-shaped points with different parameters $\theta_2 = \theta_3 = 0.4\pi$ (red star), $\theta_2 = 0.35\pi$, $\theta_3 = 0.5\pi$ (blue star) and $\theta_2 = 0.2\pi$, $\theta_3 = 0.8\pi$ (black star), respectively. Other parameters are $\lambda_a = -\lambda_b = 1$, $\eta = 3$ and $\theta_1 = 0.2\pi$.

The interchain coupling is contained in $V(k)$, which can be expressed as

$$V(k) = \begin{pmatrix} 0 & -\omega_+ \sin\lambda_a\theta_3 & -\omega_- + \omega_+ \cos\lambda_a\theta_3 & 0 \\ \omega_+ \sin\lambda_b\theta_3 & 0 & 0 & \omega_- + \omega_+ \cos\lambda_b\theta_3 \\ -\omega_- + \omega_+ \cos\lambda_b\theta_3 & 0 & 0 & -\omega_+ \sin\lambda_b\theta_3 \\ 0 & \omega_- + \omega_+ \cos\lambda_a\theta_3 & \omega_+ \sin\lambda_a\theta_3 & 0 \end{pmatrix}. \tag{19}$$

According to equations (16)–(19), we obtain the final Hamiltonian $H_{\mathrm{eff}}(k)$ by $H_{\mathrm{eff}}(k) = i\ln U(k)$.

We focus on the Floquet operator U, which is the most commonly used one for investigating discrete-time quantum walk dynamics. Despite the lack of a simple form, $H_{\mathrm{eff}}(k)$ is a non-Hermitian Hamiltonian, which features NHSE and reflects the breakdown of the conventional bulk-boundary correspondence. When governed by the non-unitary operator, the quantum walk with the directional hopping and the alternative gain–loss contributes to the nonreciprocal accumulation of population and further generates NHSE. Especially, taking the interchain coupling into account, the direction of NHSE for U_0 and U becomes different.

According to the effective Hamiltonian calculated above, we can find that some energy spectra have become complex spectra due to non-Hermiticity. Subsequently, the spectral winding number is defined as [46]

$$w = \frac{1}{2\pi}\int_0^{2\pi} \frac{\mathrm{d}}{\mathrm{d}k}\arg\left[H(k) - E_0\right]\mathrm{d}k \tag{20}$$

where $H(k)$ denotes the effective Hamiltonian of $U(k)$, and E_0 denotes a point selected in the complex energy plane. In figure 3, we show the topological phase diagram. Here the topology we refer to is the spectral topology. For blue and pink regions in figure 3, energy spectra may form a closed loop as k traverses from 0 to 2π, indicating the system is topologically nontrivial. However, energy spectra cannot enclose any region when along phase boundaries, indicating the system is topologically trivial with $w = 0$ and a vanishing NHSE which will be confirmed in the following discussion.

3.1. Numerical simulation and analysis

In the above model, the system's non-Hermiticity gradually increases the localization of the eigenstates to the boundary direction, as expected in the NHSE regime. This behavior can be easily quantified by calculating the average eigenstate localization in the form of the mean center of mass (MCOM) of the amplitude squared of all eigenvectors [79], defined as

$$\mathrm{MCOM} = \frac{\sum_{x=0}^{N}(x+1)A(x)}{\sum_{x=0}^{N}A(x)}, \tag{21}$$

where $A(x) = \frac{1}{N+1}\sum_{n=0}^{N}|\langle x|\phi_n\rangle|^2$ indicates the mean eigenvector probability amplitude with eigenvector $|\phi_n\rangle$ and $x = 0,\ldots,N$. Apparently, the MCOM can directly characterize the direction of NHSE, where the

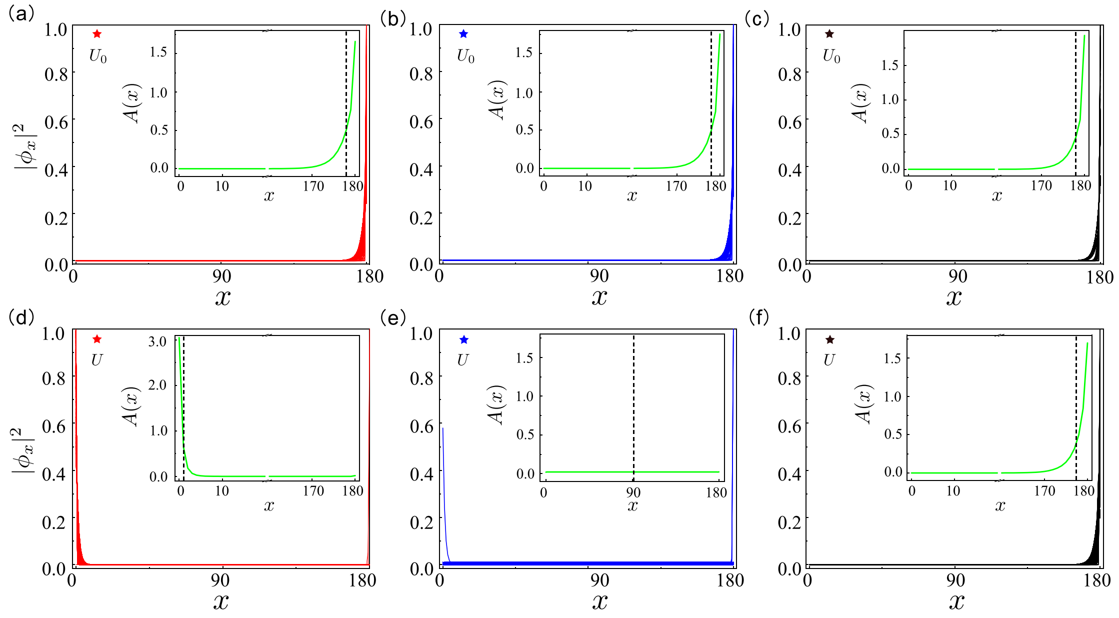

Figure 4. Spatial distribution of all eigenstates. (a)–(c) Eigenstate distributions (under OBC) of quantum walks without the interchain hopping with $\theta_2 = \theta_3 = 0.4\pi$ (red star), $\theta_2 = 0.35\pi$, $\theta_3 = 0.5\pi$ (blue star) and $\theta_2 = 0.2\pi$, $\theta_3 = 0.8\pi$ (black star), respectively. (d)–(f) Eigenstate distributions (under OBC) of quantum walks with the interchain hopping. Insets: the mean eigenvector amplitude $A(x)$ (green lines) under OBC for the two quantum walks governed by U_0 and U respectively. The vertical dashed lines indicate the MCOM in each case. Other parameters: $\lambda_a = -\lambda_b = 1$, $\eta = 3$, $\theta_1 = 0.2\pi$ and $N = 180$.

MCOM approaching to N means eigenstates are mostly accumulated on the right boundary and the MCOM approaching to 0 means eigenstates are accumulated on the left boundary. Then we plot the eigenstate distributions and MCOM under OBC in figures 4(a)–(f).

The two legs are completely decoupled when the quantum walk is governed by U_0. Since the probability of the hopping to the right for each leg is higher than that to the left, the preferred direction of the nonreciprocal hopping is right. As illustrated in figures 4(a)–(c), we can clearly see the MCOM is near the right boundary, which displays the localization of the skin eigenmodes near the right edge.

Once the interchain coupling is turned on, both the complex spectra and the eigenmodes of the coupled system behave differently from those of the uncoupled ones, as shown in figures 3 and 4. As the quantum walk is governed by U, the direction of eigenmode accumulation is reversed, the MCOM moves near the left boundary and the eigenmodes are accumulated to the left boundary, as shown by the eigenmode distributions in figure 4(d). As a comparison, eigenstate distributions corresponding to the other two cases are also plotted in figures 4(e) and (f). There is no skin effect inversion in figure 4(f) and an absence of NHSE in figure 4(e). However, we can see that once the interchain coupling is introduced, eigenstates gradually begin to accumulate towards the boundary opposite to the preferred NHSE direction and the MCOM starts moving from right to left, and even the disappearance of NHSE occurs during this process. This further suggests that the reversed NHSE can be generated by introducing interchain couplings. However, there is a limit to its strength. The direction of NHSE completely reverses only when coupling strength exceeds the limit.

The evolved state after t step is expressed as $|\Phi_t\rangle = \sum_{x,y=a,b,u=0,1} \phi_t^{x,y,u}|y,x\rangle \otimes |u\rangle$. To determine the direction of photons accumulation, we consider the normalized spatial distributions

$$P_t(x) = \sum_{y=a,b,u=0,1} \left|\tilde{\phi}_t^{x,y,u}\right|^2 = \sum_{y=a,b,u=0,1} \left|\frac{\phi_t^{x,y,u}|y,x\rangle \otimes |u\rangle}{\sqrt{\sum_{x,y=a,b,u=0,1} |\phi_t^{x,y,u}|^2}}\right|^2, \tag{22}$$

where $\tilde{\phi}_t^{x,y,u}$ is the normalized final state. We now numerically analyze the direction of particle accumulation of the quantum walks governed by U_0 and U, respectively. Subsequently, the normalized spatial probability distribution $P_t(x)$ for U_0 or U is numerically shown in figures 5(a) and (b). The reversed NHSE can be observed in the quantum walk with a finite number of steps, which is extremely friendly and convenient for experimental realization. Next, we consider the quantum walk with two legs, whose position x only takes 0 or 1. To eliminate the effect of the oscillatory dynamics under a finite system size, we take a time average of the spatial distribution here, $P_t(x) = \frac{1}{t}\sum_{\tau=1}^{t} P_\tau(x)$. Through numerical simulations, we can obtain the

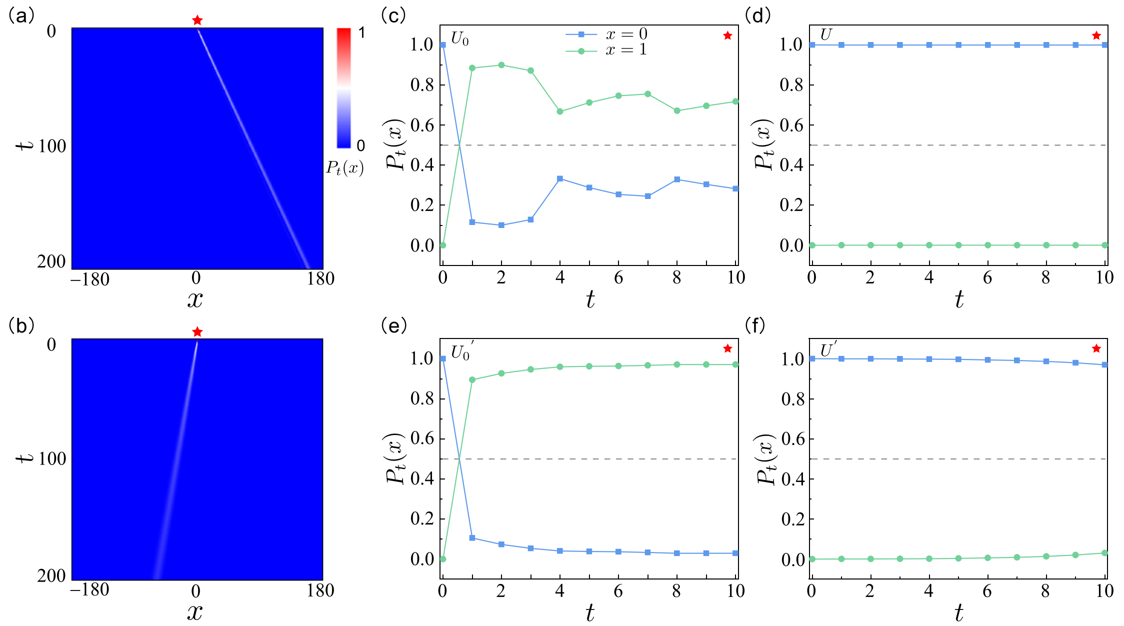

Figure 5. Normalized spatial distribution. The normalized spatial probability distributions $P_t(x)$ for U_0 (a) and U (b), respectively. (c)–(f) Numerical results of the normalized spatial distribution $P_t(x)$ for a quantum walk scheme governed by U_0 and U, with two lattice positions and total time steps $t=10$, (i.e. x only takes 0 or 1). Different from (c), (d), for $U_0^{'}$ and $U^{'}$ we switch the positions of S_1 and S_2 in U_0 and U in (e), (f). The initial state of the system is prepared as $|\Phi_0\rangle = (|a,0\rangle\otimes|H\rangle + |b,0\rangle\otimes|H\rangle)/\sqrt{2}$. Other parameters: $\theta_2=\theta_3=0.4\pi$, $\lambda_a=-\lambda_b=1$, $\eta=3$ and $\theta_1=0.2\pi$.

probabilities of the walker being at $x=0$ and 1 for both legs. From figure 5(c), we can observe that the nonreciprocal accumulation mostly localizes to the right boundary $x=1$ which indicates the existence of NHSE induced by U_0. Compared with U_0, the direction of this nonreciprocal accumulation is reversed when the system is governed by U in figure 5(d). This clearly indicates the direction of the NHSE is reversed when introducing the interchain coupling by S_3 and S_4. Meanwhile, over a longer evolution, we find the reversed NHSE is consistently dominant, as depicted in figures 5(a) and (b). In such a small system under the OBC, whether S_1 or S_2 acts first in the Floquet operator may also affect the results. To exclude the effect on the reversal of NHSE, we can switch the positions of S_1 and S_2 in Floquet operators. Numerical simulation in figures 5(e) and (f) shows that the reversal of NHSE still appears and has nothing to do with S_1 and S_2, which further proves that it is indeed the result of interchain couplings.

For better characterizing the direction of particle accumulation, we further define the average position occupation of the final state as $\bar{x}_t = \sum_{x,y=a,b,u=0,1} x\,|\tilde{\phi}_t^{x,y,u}|^2$. By fixing $\theta_1 = 0.2\pi$ and $x=0$, after a long time evolution, we calculate the deviation of the final average position for the two quantum walks governed by U_0 and U under OBC

$$\Delta = \frac{1}{2N}|\bar{x}_{U_0} - \bar{x}_U|, \tag{23}$$

which reflects the strength of reverse accumulation and visually displays the degree of reversed NHSE. A phase diagram versus two rotation angles θ_2 and θ_3 is shown in figure 6. We find that θ_2 and θ_3 may represent the coupling strength and further control the degree of particle reverse accumulation. The phase boundary of this diagram is as same as that in figure 3, further indicating the topological phase diagram is experimentally accessible by measuring Δ.

3.2. Experimental proposal

Based on the idea of linear optical realization of quantum walks on a ladder in figure 2, the experimental scheme for the demonstration of reversed NHSE via quantum walks is illustrated in figure 7. The walker's position x only takes 0 or 1. The whole scheme is mainly composed of three parts: preparation of system initial state, implementation of non-unitary Floquet operator, and measurement. The heralded single photons can be generated via type-I spontaneous parametric down-conversion in a β-barium-borate (BBO) nonlinear crystal, pumped by a CW diode laser. As discussed above, we can also implement the required rotation operator with one or two wave plates. Here we prepare the initial state $|\Phi_0\rangle = (|a,0\rangle\otimes|H\rangle + |b,0\rangle\otimes|H\rangle)/\sqrt{2}$. Taking this quantum walk driven by U_0 and U with $2\theta_1=\theta_2=\theta_3=0.4\pi$ as an example, we list the angles of the wave plates in figure 7.

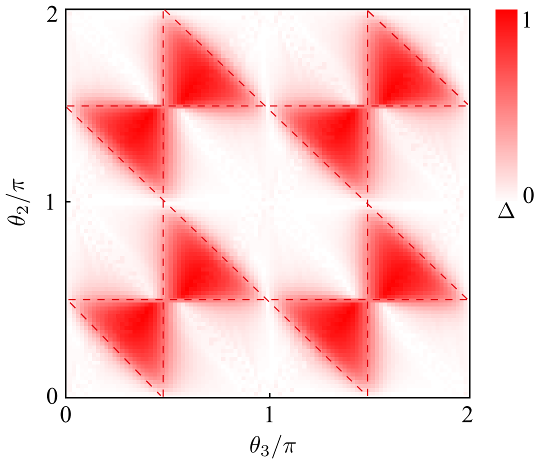

Figure 6. The deviation Δ of the final average position for the two quantum walks. Quantum walks governed by U_0 and U, respectively, under OBC at total time step $t = 40$ versus the two angles θ_2 and θ_3. Here the particle position starts at $x = 0$ and is limited to hopping between $x = N$ and $x = -N$. We can see that the darker the color, the more obvious the degree of reverse accumulation. These dashed lines represent approximate boundaries. Other parameters: $\lambda_a = -\lambda_b = 1$, $\eta = 3$, $\theta_1 = 0.2\pi$ and $N = 10$.

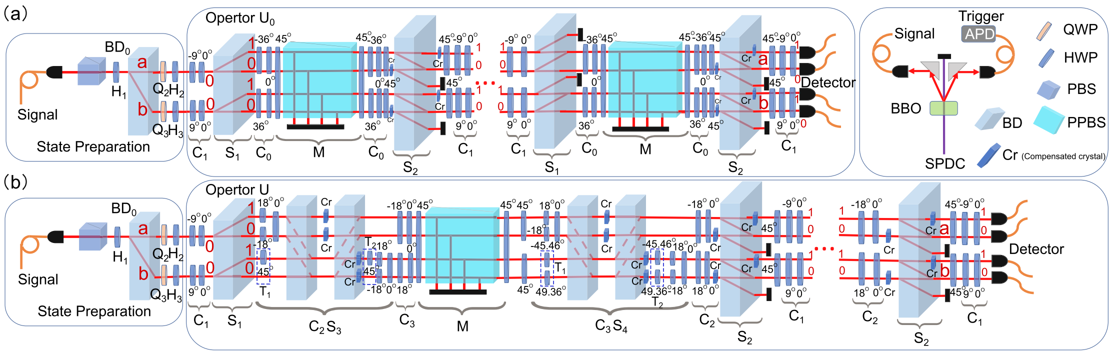

Figure 7. Schematic of experimental setup for reversed NHSE. Photon pairs are generated via spontaneous parametric down-conversion (SPDC). One of these yielded pairs of photons is heralded as a signal photon into the subsequent interferometric network, the other serves as a trigger. Here BD$_0$ is used to stratify the leg into upper and lower legs. We define the upper path as the leg a and the lower as the leg b, respectively. Two non-unitary evolutions U_0 (a) and U (b) are realized by a set of wave plates and an interferometer involving two BDs. After state preparation, the solid lines inside BDs represent their respective intrachain hopping for each leg, and dotted lines represent interchain hopping between two legs. Photons beyond positions 0 and 1 and lost from the PPBS are collected by APDs (black boxes). Finally, output photons are detected by APDs after every time step.

For the Floquet operator U_0, the coin rotation operator $C(\theta)$ can be realized by HWPs. It should be noted that the optical axes of the BDs realizing the shift operators S_1 and S_2 should be perpendicular to that of the first BD$_0$. After passing through BD$_0$, the photons on each leg are independently divided into the front and back paths, realizing photons' hopping between position 0 and 1 for each leg. Especially, when realizing the shift operator S_2 which controls the hopping of photons only in a vertically polarized state, we can operate it by using an HWP at 45° to turn $|V\rangle$ into $|H\rangle$, and then add the same HWP for transformation back. To distinguish the direction of particle propagation, the system must evolve under the OBC. Thus, photons that hop out of the boundary escape from the systems. But we still need to collect these photons to monitor the experimental efficiency.

The non-unitarity operator M is implemented by a partially PBS (PPBS), whose effect is characterized as a selective-loss operator $M_\mathrm{E} = \sum_x \sum_{y=a,b} |y,x\rangle\langle y,x| \otimes (|H\rangle\langle H| + \sqrt{1-p}|V\rangle\langle V|)$ with $0 \leqslant p \leqslant 1$, realizing a partial measurement at every time step. Thus, we obtain the map $M = QM_\mathrm{E}Q$, with $\eta = -\frac{1}{2}\ln(1-p)$ and the matrix $Q = \sum_x \sum_{y=a,b} |y,x\rangle\langle y,x| \otimes \sigma_1$. The Pauli matrix σ_1 can be realized by an HWP at 45°. To have the complete quantum channel map, a second Kraus operator is present, specifically $M_{\bar{\mathrm{E}}} = \sum_x \sum_{y=a,b} |y,x\rangle\langle y,x| \otimes \sqrt{p}|V\rangle\langle V|$. In this way, $M_\mathrm{E}^\dagger M_\mathrm{E} + M_{\bar{\mathrm{E}}}^\dagger M_{\bar{\mathrm{E}}} = \mathbb{1}$. Hence, to monitor non-unitarity dynamics, one then can collect the photons lost due to the effect of operator M_E and compare analytically them with the photons that pass through at each time step.

The experimental implementation of the Floquet operator U is similar to that of U_0 except for interchain shift operators S_3 and S_4, as shown in figure 7(b). The implementation of S_3 or S_4 needs to consider both $S_\uparrow$ and $S_\downarrow$. To realize the mutual interchain hopping between two legs, two BDs are respectively needed to achieve S_3 or S_4, and the design of the optical path also needs to be combined with coin rotation operators C_2 and C_3. Here we consider step-by-step implementation. First, we realize the hopping from leg a to leg b and then realize the hopping from leg b to leg a. During this process, we just rotate the related HWPs' angles corresponding to the operator T_1 to make the photons' polarization states completely into $|V\rangle$. After passing through two BDs the operator T_2 is used to transform the polarization of the photons back to the original polarization states. We find the setting angles of these wave plates to implement T_2 and T_1 are same. When realizing the shift operator S_2 and S_4 which controls the hopping of photons only in a vertically polarized state, we can operate it by using an HWP at 45° to turn $|V\rangle$ into $|H\rangle$, and finally add the same HWP for transformation back. Through the operators S_1 and S_2, photons beyond positions 0 and 1 will be lost and collected. Thus in such a small system under the OBC, whether S_1 or S_2 acts first in the Floquet operator may affect the reversal of NHSE. To exclude their effect, we can switch the positions of S_1 and S_2, adjust the angles of partial wave plates as needed and perform a contrast experiment.

Finally, after every time step photons are detected by four APDs, recording photons coincidence events. Then we can obtain the number of photons at different positions, $n_t^{a,0}$, $n_t^{a,1}$, $n_t^{b,0}$, $n_t^{b,1}$ and their sum is the total number of photons n_t after t steps. Experimentally, we can obtain $P_t(x) = (\sum_{y=a,b} n_t^{u,x})/n_t$ and $\bar{x}_t = x(\sum_{u=a,b} n_t^{u,x})/n_t$. Based on the two observable quantities, we can observe the accumulation direction and inversion degree of particles, and simulate the phase diagram, further demonstrating the feasibility of the experimental scheme. It needs to be emphasized that this experimental scheme can be easily extended to higher lattice space, we can take advantage of the lattice position after the black boxes in figure 7 and the design can be based on the quantum walks on a ladder at positions $x = -N\ldots N$ in figure 2.

4. Conclusion

In this paper, we propose an experimental scheme to demonstrate quantum walks on a ladder in optical systems. This scheme is concrete and feasible because it is mainly based on linear optical elements which are easily regulated. As an application, we also propose an experimental scheme to demonstrate the direction reversal of NHSE using quantum walks on a two-leg ladder. Our approach is to use the photonic quantum walk platform to simulate the quantum dynamics of a one-dimensional double-chain non-Hermitian quasicrystal with interchain coupling. We calculate the effective Hamiltonian of the quantum walk and corresponding mean center of mass of eigenmodes, which can intuitively characterize the evolution behavior of quantum systems in nature. Through numerical simulations, we find that for the non-unitary quantum walk on a ladder with two legs, the direction of photon accumulation is opposite to the preferred nonreciprocal accumulation direction of previously decoupled both legs when the interchain hopping is introduced. Due to the existence of loss in the system, this particle nonreciprocal accumulation is the manifestation of NHSE. Our scheme thus unveils a physical phenomenon of direction reversal of NHSE existing in non-Hermitian systems with interchain coupling. This may provide a feasible route for the development and application of techniques from non-Hermitian and nonreciprocal physics.

Data availability statement

All data that support the findings of this study are included within the article (and any supplementary files).

Acknowledgment

This work has been supported by the National Natural Science Foundation of China (Grant Nos. 92265209 and 12025401). K K W acknowledges support from the National Natural Science Foundation of China (Grant No. 12104009). L X acknowledges support from the National Natural Science Foundation of China (Grant No. 12104036). H Q L acknowledges support from the National Natural Science Foundation of China (Grant No. 12088101).

Conflict of interest

The authors declare that there are no competing interests.

Author contributions

X W W conceived the ideas with contributions from L X, Q L, K K W and H Q L. X W W performed numerical simulations. P X supervised the work and all authors contributed to writing the paper.

ORCID iD

Peng Xue https://orcid.org/0000-0002-4272-2883

References

[1] Aharonov Y, Davidovich L and Zagury N 1993 Quantum random walks *Phys. Rev.* A **48** 1687

[2] Meyer D A 1996 From quantum cellular automata to quantum lattice gases *J. Stat. Phys.* **85** 551

[3] Shenvi N, Kempe J and Whaley K B 2003 Quantum random-walk search algorithm *Phys. Rev.* A **67** 052307

[4] Ambainis A 2004 Quantum search algorithms *ACM SIGACT News* **35** 22

[5] Childs A M 2009 Universal computation by quantum walk *Phys. Rev. Lett.* **102** 180501

[6] Wang B, Chen T and Zhang X 2018 Experimental observation of topologically protected bound states with vanishing Chern numbers in a two-dimensional quantum walk *Phys. Rev. Lett.* **121** 100501

[7] Zhang W W, Sanders B C, Apers S, Goyal S K and Feder D L 2017 Detecting topological transitions in two dimensions by Hamiltonian evolution *Phys. Rev. Lett.* **119** 197401

[8] Schreiber A, Cassemiro K N, Potoček V, Gábris A, Jex I and Silberhorn C 2011 Decoherence and disorder in quantum walks: from ballistic spread to localization *Phys. Rev. Lett.* **106** 180403

[9] Crespi A, Osellame R, Ramponi R, Giovannetti V, Fazio R, Sansoni L, Nicola F D, Sciarrino F and Mataloni P 2013 Anderson localization of entangled photons in an integrated quantum walk *Nat. Photon.* **7** 322

[10] Edge J M and Asboth J K 2015 Localization, delocalization and topological transitions in disordered two-dimensional quantum walks *Phys. Rev.* B **91** 104202

[11] Schmitz H, Matjeschk R, Schneider C, Glueckert J, Enderlein M, Huber T and Schaetz T 2009 Quantum walk of a trapped ion in phase space *Phys. Rev. Lett.* **103** 090504

[12] Alberti A, Alt W, Werner R and Meschede D 2014 Decoherence models for discrete-time quantum walks and their application to neutral atom experiments *New J. Phys.* **16** 123052

[13] Broome M A, Fedrizzi A, Lanyon B P, Kassal I, Aspuru-Guzik A and White A G 2010 Discrete single photon quantum walks with tunable decoherence *Phys. Rev. Lett.* **104** 153602

[14] Schreiber A, Cassemiro K N, Potoček V, Gábris A, Mosley P J, Andersson E, Jex I and Silberhorn C 2010 Photons walking the line: a quantum walk with adjustable coin operations *Phys. Rev. Lett.* **104** 050502

[15] Wang K, Qiu X, Zhan X, Bian Z H, Yi W and Xue P 2019 Simulating dynamic quantum phase transitions in photonic quantum walks *Phys. Rev. Lett.* **122** 020501

[16] Xiao L, Deng T, Wang K, Zhu G, Wang Z, Yi W and Xue P 2020 Non-Hermitian bulk–boundary correspondence in quantum dynamics *Nat. Phys.* **16** 761

[17] Zhang R, Hou Z, Li Z, Zhu H, Xiang G, Li C and Guo G 2021 Experimental masking of real quantum states *Phys. Rev. Appl.* **16** 024052

[18] Ali H and Shahid M N 2020 Quantum walk on a ladder (arXiv:2012.13994)

[19] Poulios K *et al* 2014 Quantum walks of correlated photon pairs in two-dimensional waveguide arrays *Phys. Rev. Lett.* **112** 143604

[20] Huang F T, Xue F, Gao B, Wang L H, Luo X, Cai W, Lu X Z, Rondinelli J M, Chen L Q and Cheong S W 2016 Domain topology and domain switching kinetics in a hybrid improper ferroelectric *Nat. Commun.* **7** 11602

[21] Gräfe M and Szameit A 2020 Integrated photonic quantum walks *J. Phys. B: At. Mol. Opt. Phys.* **53** 073001

[22] Kitagawa T, Rudner M S, Berg E and Demler E 2010 Exploring topological phases with quantum walks *Phys. Rev.* A **82** 033429

[23] Boada O, Novo L, Sciarrino F and Omar Y 2017 Quantum walks in synthetic gauge fields with three-dimensional integrated photonics *Phys. Rev.* A **95** 013830

[24] D'Errico A, Cardano F, Maffei M, Dauphin A, Barboza R, Esposito C, Piccirillo B, Lewenstein M, Massignan P and Marrucci L 2016 Two-dimensional topological quantum walks in the momentum space of structured light *Optica* **7** 108

[25] Chen C, Ding X, Qin J, Wu J, He Y, Lu C, Li L, Liu X, Sanders B C and Pan J 2022 Topological spin texture of chiral edge states in photonic two-dimensional quantum walks *Phys. Rev. Lett.* **129** 046401

[26] Meyer-Scott E, Prasannan N, Eigner C, Quiring V, Donohue J M, Barkhofen S and Silberhorn C 2018 High-performance source of spectrally pure, polarization entangled photon pairs based on hybrid integrated-bulk optics *Opt. Express* **26** 32475

[27] Bender C M and Boettcher S 1998 Real spectra in non-Hermitian Hamiltonians having PT symmetry *Phys. Rev. Lett.* **80** 5243

[28] Bender C M, Brody D C and Jones H F 2002 Complex extension of quantum mechanics *Phys. Rev. Lett.* **89** 270401

[29] Bender C M, Brody D C and Jones H F 2003 Must a Hamiltonian be Hermitian? *Am. J. Phys.* **71** 1095

[30] Bender C M 2007 Making sense of non-Hermitian Hamiltonians *Rep. Prog. Phys.* **70** 947

[31] Rotter I A 2009 Non-Hermitian Hamilton operator and the physics of open quantum systems *J. Phys. A: Math. Theor.* **42** 153001

[32] Shen H and Fu L 2018 Quantum oscillation from in-gap states and a non-Hermitian Landau level problem *Phys. Rev. Lett.* **121** 026403

[33] Klaiman S, Günther U and Moiseyev N 2008 Visualization of branch points in PT-symmetric waveguides *Phys. Rev. Lett.* **101** 080402

[34] Longhi S 2009 Bloch oscillations in complex crystals with PT symmetry *Phys. Rev. Lett.* **103** 123601

[35] Malzard S, Poli C and Schomerus H 2015 Topologically protected defect states in open photonic systems with non-Hermitian charge-conjugation and parity-time symmetry *Phys. Rev. Lett.* **115** 200402

[36] Xiao L *et al* 2017 Observation of topological edge states in parity–time-symmetric quantum walks *Nat. Phys.* **13** 1117

[37] Zhou H, Peng C, Yoon Y, Hsu C W, Nelson K A, Fu L, Joannopoulos J D, Soljačić M and Zhen B 2018 Observation of bulk Fermi arc and polarization half charge from paired exceptional points *Science* **359** 1009

[38] Ding K, Ma G, Zhang Z Q and Chan C T 2018 Experimental demonstration of an anisotropic exceptional point *Phys. Rev. Lett.* **121** 085702

[39] Xiao L, Wang K, Zhan X, Bian Z, Kawabata K, Ueda M, Yi W and Xue P 2019 Observation of critical phenomena in parity-time-symmetric quantum dynamics *Phys. Rev. Lett.* **123** 230401

[40] Tang W, Jiang X, Ding K, Xiao Y X, Zhang Z Q, Chan C T and Ma G 2020 Exceptional nexus with a hybrid topological invariant *Science* **370** 1077

[41] Zhang Z *et al* 2020 Tunable topological charge vortex microlaser *Science* **368** 760

[42] Ji Z, Liu W, Krylyuk S, Fan X, Zhang Z, Pan A, Feng L, Davydov A and Agarwal R 2020 Photocurrent detection of the orbital angular momentum of light *Science* **368** 763

[43] Rivero J D H, Pan M, Makris K G, Feng L and Ge L 2021 Non-Hermiticity-governed active photonic resonances *Phys. Rev. Lett.* **126** 163901

[44] Zhang X, Zhang T, Lu M and Chen Y 2022 A review on non-Hermitian skin effect *Adv. Phys.* X **7** 2109431

[45] Yao S and Wang Z 2018 Edge states and topological invariants of non-Hermitian systems *Phys. Rev. Lett.* **121** 086803

[46] Zhang K, Yang Z and Fang C 2020 Correspondence between winding numbers and skin modes in non-Hermitian systems *Phys. Rev. Lett.* **125** 126402

[47] Yang Z, Zhang K, Fang C and Hu J 2020 Non-Hermitian bulk-boundary correspondence and auxiliary generalized Brillouin zone theory *Phys. Rev. Lett.* **125** 226402

[48] Song F, Yao S and Wang Z 2019 Non-Hermitian skin effect and chiral damping in open quantum systems *Phys. Rev. Lett.* **123** 170401

[49] Borgnia D S, Kruchkov A J and Slager R J 2020 Non-Hermitian boundary modes and topology *Phys. Rev. Lett.* **124** 056802

[50] Okuma N, Kawabata K, Shiozaki K and Sato M 2020 Topological origin of non-Hermitian skin effects *Phys. Rev. Lett.* **124** 086801

[51] Longhi S 2021 Non-Hermitian skin effect beyond the tight-binding models *Phys. Rev.* B **104** 125109

[52] Yokomizo K and Murakami S 2021 Scaling rule for the critical non-Hermitian skin effect *Phys. Rev.* B **104** 165117

[53] Li L, Lee C H, Mu S and Gong J 2020 Critical non-Hermitian skin effect *Nat. Commun.* **1** 5491

[54] Mu S, Zhou L, Li L and Gong J 2022 Non-Hermitian pseudo mobility edge in a coupled chain system *Phys. Rev.* B **105** 205402

[55] Kawabata K, Sato M and Shiozaki K 2020 Higher-order non-Hermitian skin effect *Phys. Rev.* B **102** 205118

[56] Guo C X, Liu C H, Zhao X M, Liu Y and Chen S 2021 Exact solution of non-Hermitian systems with generalized boundary conditions: size-dependent boundary effect and fragility of the skin effect *Phys. Rev. Lett.* **127** 116801

[57] Ghorashi S A A, Li T and Sato M 2021 Non-Hermitian higher-order Weyl semimetals *Phys. Rev.* B **104** L161117

[58] Zhang K, Yang Z and Fang C 2022 Universal non-Hermitian skin effect in two and higher dimensions *Nat. Commun.* **13** 2496

[59] Weidemann S, Kremer M, Helbig T, Hofmann T, Stegmaier A, Greiter M, Thomale R and Szameit A 2020 Topological funneling of light *Science* **368** 311

[60] Zhang X, Tian Y, Jiang J H, Lu M H and Chen Y F 2021 Observation of higher-order non-Hermitian skin effect *Nat. Commun.* **12** 5377

[61] Zou D, Chen T, He W, Bao J, Lee C H, Sun H and Zhang X 2021 Observation of hybrid higher-order skin-topological effect in non-Hermitian topolectrical circuits *Nat. Commun.* **12** 7201

[62] Lin Q, Li T, Xiao L, Wang K, Yi W and Xue P 2022 Topological phase transitions and mobility edges in non-Hermitian quasicrystals *Phys. Rev. Lett.* **129** 113601

[63] Lin Q, Li T, Xiao L, Wang K, Yi W and Xue P 2022 Observation of non-Hermitian topological Anderson insulator in quantum dynamics *Nat. Commun.* **13** 3229

[64] Li L, Teo W X, Mu S and Gong J 2022 Direction reversal of non-Hermitian skin effect via coherent coupling *Phys. Rev.* B **106** 08547

[65] Wanjura C C, Brunelli M and Nunnenkamp A 2020 Topological framework for directional amplification in driven-dissipative cavity arrays *Nat. Commun.* **11** 3149

[66] Xue W T, Li M R, Hu Y M, Song F and Wang Z 2021 Simple formulas of directional amplification from non-Bloch band theory *Phys. Rev.* B **103** L241408

[67] Lu L, Joannopoulos J D and Soljačić M 2014 Topological photonics *Nat. Photon.* **8** 821

[68] Zhang X, Xiao M, Cheng Y, Lu M H and Christensen J 2018 Topological sound *Commun. Phys.* **1** 97

[69] Ghataka A, Brandenbourgera M, Wezela J V and Coulaisa C 2020 Observation of non-Hermitian topology and its bulk–edge correspondence in an active mechanical metamaterial *Proc. Natl Acad. Sci. USA* **117** 29561

[70] Xiao L, Deng T, Wang K, Wang Z, Yi W and Xue P 2021 Observation of non-Bloch parity-time symmetry and exceptional points *Phys. Rev. Lett.* **126** 230402

[71] Wang K, Li T, Xiao L, Han Y, Yi W and Xue P 2021 Detecting non-Bloch topological invariants in quantum dynamics *Phys. Rev. Lett.* **127** 270602

[72] Bru L A, Valcárcel G J D, Molfetta G D, Pérez A, Roldán E and Silva F 2016 Quantum walk on a cylinder *Phys. Rev.* A **94** 032328

[73] Aharonov D, Ambainis A, Kempe J and Vazirani U 2001 Quantum walks on graphs *Proc. 33rd Annual ACM Symp. on Theory of Computing STOC'01* pp 50–59

[74] Shalm L K *et al* 2015 Strong loophole-free test of local realism *Phys. Rev. Lett.* **115** 250402

[75] Wang Y, Li Z, Yu S, Ke Z, Liu W, Meng Y, Yang Y, Tang J, Li C and Guo G 2020 Experimental investigation of state distinguishability in parity-time symmetric quantum dynamics *Phys. Rev. Lett.* **124** 230402

[76] Chaturvedi S, Marmo G, Mukunda N, Simon R and Zampini A 2006 The Schwinger representation of a group: concept and applications *Rev. Math. Phys.* **18** 887

[77] Reck M, Zeilinger A, Bernstein H J and Bertani P 1994 Experimental realization of any discrete unitary operator *Phys. Rev. Lett.* **73** 58

[78] Clements W R, Humphreys P C, Metcalf B J, Kolthammer W S and Walsmley I A 2016 Optimal design for universal multiport interferometers *Optica* **3** 1460

[79] Molignini P, Arandes O and Bergholtz E J 2023 Anomalous skin effects in disordered systems with a single non-Hermitian impurity (arXiv:2302.09081)